https://dx.doi.org/10.1016/j.bpj.2021.05.010

Biophysical Properties of Corneal Cells Reflect High Myopia Progression

Y. Xin, B. S. Kang, Y-P. Zheng, S. W. Shan, C-S. Kee, Y. Tan

Running Title: Biophysics of Corneal cells in Myopia

Keywords: biophysical property, cornea, myopia.

Abstract

Myopia is a common ocular disorder with significant alterations in the anterior ocular structure, including the cornea. The cell biophysical phenotype has been proposed to reflect the state of various diseases. However, the biophysical properties of corneal cells have not been characterized during myopia progression and their relationship with myopia remains unknown. This study characterizes the biophysical properties of corneal cells in normal, myopic, and recovered conditions, using two classical myopia models. Surprisingly, myopic corneal cells considerably reduce F-actin/microtubule content and cellular stiffness and generate elevated traction force compared to control cells. When myopia is restored to the healthy state, these biophysical properties are partially/fully restored to the levels of control cells. Furthermore, the level of chromatin condensation is significantly increased in the nucleus of myopic corneal cells and reduced to a level similar to healthy cells after recovery. These findings demonstrate that the reversible biophysical alterations of corneal cells reflect myopia progression, facilitating the study of the role of corneal cell biophysics in myopia.

Introduction

As one of the most common ocular disorders, myopia affects over 22% of the population worldwide (1, 2). Of particular concern is the increasing prevalence of high myopia, because of the structural anomalies of the abnormally long eyeball (3) and its association with sight-threatening pathological conditions (4). Although genetic and environmental factors have been identified to be involved in myopia initiation and progression (5), the mechanisms underlying this disorder remain unclear. Numerous human and animal studies have demonstrated significant changes in ocular biometrics of the posterior segment of the eye in high myopes, including scleral thinning and vitreous chamber elongation. However, very little is known about how high myopia progression alters anterior ocular biometrics (5). As the anterior connective tissue of the eye, the cornea contributes more than 60% of focusing power and is the primary target for refractive correction (3). Therefore, it is important to characterize alterations in corneal properties at both tissue and cellular levels.

In addition to biochemical factors, biophysical cues play important roles in various pathological processes (6, 7). In particular, mechanical alterations of cells accompany the onset and progression of a wide range of disorders, including glaucoma (8), solid tumor (9), leukemia (10), malaria (11), and cardiovascular diseases (12), and influence cellular functions and disease development through mechanotransduction (13). Importantly, the biophysical phenotype of living cells reflects the status of many disorders and may serve as a biomarker for disease diagnosis and prognosis. Thus, characterizing the biophysical properties of the relevant cells is crucial to unveil the significance of biomechanics. Accumulating evidence has demonstrated notable alterations in structural and mechanical properties of corneal tissues in myopia and other ocular disorders (14-17). As the basic unit, living cells and their properties influence the structure and function of the constituted tissues. Cell mechanics are pivotal in

regulating cellular functions and reflect the developmental stage of various human diseases. Cellular stiffness serves as a biomechanical stemness indicator of corneal limbal stem cells (18). Substrate stiffness regulates the morphology and generation of contractile force of corneal keratocytes in the presence of TGF-β1 (19). However, the mechanics of corneal cells have not been well characterized in myopia. Whether and how these cellular biophysical alterations relate to myopia progression remains unknown.

In this study, cellular biophysical properties, including cytoskeleton, cell mechanics, and traction force, and chromatin condensation were characterized in corneal cells under normal, myopic, and recovered conditions. It was found that corneal cells exhibited reduced F-actin/microtubule content and cellular stiffness with elevated cellular traction force and chromatin condensation in the myopic state. Both cellular biophysical properties and chromatin condensation were restored to the levels of normal corneal cells in the restored eyes. The reversible changes indicate that biophysical properties of corneal cells reflect myopia progression and may be involved in the pathological process.

Materials and Methods

Animal Ethics. All animal experiments in this study were performed on White Leghorn chicks (*Gallus gallus domesticus*) raised in the Centralized Animal Facility of the University. Chicks were kept in a temperature-controlled room with a 12 hr:12 hr light-dark cycle and unlimited access to food and water. The adopted experimental protocols were approved by the University Animal Subjects Ethics Sub-Committee (ASESC 17-18/51) and conformed to the ARVO Statement for the Use of Animals in Ophthalmic and Vision Research.

Myopia Induction.

Experiment I: *Myopia vs. Control.* Two groups of five-day-old chicks (n=8 per group) were monocularly fitted with either plastic-molded translucent occluders for 7 days to induce form-deprivation myopia (FDM), or –15 D lenses (PMMA contact lens; Conforma, U.S.) for 14 days to induce lens-induced myopia (LIM). Fellow untreated eyes served as contralateral controls. At the end of the treatment, refractive states were measured using a modified Hartinger refractometer under anesthesia (1.5% isoflurane) (20). Three repeated recordings were performed and spherical equivalent (the average of refractive errors in the two principal meridians) was used for data analysis. The induction of high myopia was conducted *in vivo*.

Experiment II: Myopia-recovery vs. Control. Two groups of five-day-old chicks (n=8 per group) received either monocular FDM or LIM as described above. At the end of the treatment, occluders/lenses were removed to allow eyes to recover from myopia with unrestricted vision for two days. Refractive states were measured at the end of the occluder- or lens-wear and two days after recovery. The induction of recovery was conducted *in vivo*.

Cornea Extraction and Cell Preparation. Chicks were euthanized by carbon dioxide asphyxiation before the occluders or lenses were removed. Both eyes were enucleated and hemisected along the ora serrata using a razor blade. Anterior segment tissues, excluding cornea (iris, ciliary body, and crystalline lens), were gently removed and washed in chilled-phosphate buffered saline (PBS). Then a sterilized Biopsy Punch (Integra™, Miltex, U.S.) was used to collect a 4-mm diameter sample of the central corneal tissues. The whole process took ~1 h. Samples were predigested by rinsing with sterile 0.1% collagenase (Sigma-Aldrich, U.S.) in PBS for 5 min at 37 °C. Digestion continued after replacing the collagenase solution with fresh 0.1% collagenase and shaking at 37 °C for a further 45 min. The digest was then filtered through a 40 μm nylon cell strainer (Falcon, Corning, U.S.) to remove any remaining clumps and the cells were then centrifuged at 1500 rpm for 5 min. The cell pellet was re-suspended in

Dulbecco's modified Eagle's medium (DMEM) containing 15% fetal bovine serum and 1% penicillin-streptomycin (Thermo Fisher Scientific, U.S.). It took roughly 1 h to extract the cells from the corneal tissue.

Cell Stiffness Measurement by Atomic Force Microscopy. Cell stiffness was measured by an atomic force microscope (AFM) (Bruker Catalyst) used together with an inverted microscope (Nikon). Corneal cells were seeded on a gelatin coated culture dish and incubated at 37°C for 12 h before the stiffness measurement. Soft silicon nitride cantilevers and tips with the spring constant of 0.02 N/m (MLCT, Bruker) were used as the AFM probe. The probe sensitivity and spring constant were calibrated in culture medium based on thermal vibration of the cantilever before the experiment. Corneal cells were visualized under the microscope and the cells were indented in the places around the middle of the distance between the cell periphery and the nucleus. Five different sites near the indentation area were chosen to obtain the force-indentation curves and the cell stiffness values obtained were averaged. To avoid cell damage and substrate effect, the indentation depth was kept within 500 nm and cell strain in the indentation direction was thus around 10%. The tip velocity was 1 μm/s at room temperature. For each condition, at least 50 cells were measured, and the cell Young's modulus was determined by fitting the force-indentation curves with Sneddon's model, in which a finite indenter was assumed to interact with a semi-finite, homogenous, and elastic sample (21). Cells are intrinsically viscoelastic and can be assumed to display linear elasticity under small cell strain (within 10-15%) and low loading rate (1 μm/s) during the measurement.

Traction Force Microscopy. Cellular traction force was measured using a previously published procedure (22, 23). In brief, corneal cells were sparsely seeded on 8 kPa polyacrylamide gels (~80 μm in gel thickness) with 0.2 μm red fluorescence beads embedded in the gel surface for 24 h before the traction force measurement. Images of the red fluorescence

were taken by an inverted Nikon fluorescence microscope with a 20x objective. Bright field images of cells were captured to show the cell contours. The fluorescent images of red beads beneath the cells were taken before and after trypsinizing the cells from the gels, which were used to compute the displacements of the beads and then generate a displacement field of the measured cell. Cell traction was calculated from the displacement map of the beads by the customized MATLAB program based on the inverse Boussinesq mathematical model, which is shared in the Supporting Material.

Calculation of Chromatin Condensation Parameter. To examine chromatin condensation, we measured chromatin condensation parameter following the method reported elsewhere(24). In brief, corneal cells were plated in confocal dishes (NEST Scientific USA) and fixed using 4% formaldehyde (Sigma Aldrich) for 15 min at room temperature. ProLong Gold Antifade Mountant with 4′,6-diamidino-2-phenylindole (DAPI) (Thermo-Fisher) was added to stain the nucleus. For each condition, at least 30 cells were imaged using a confocal microscope Leica DMi8 (Leica) with 63×/1.3 oil objective in the DAPI channel. The cross section of the cell nucleus was captured. The CCP was measured by the gradient-based Sobel edge detection algorithm using the enclosed MATLAB code, which was provided in the Supporting Material. In brief, to reduce the influence of fluorescence intensity, each pixel intensity of the image was divided by the maximum intensity of the image and then multiplied by 255 that was the maximum intensity for 8-bit images. Then the image was processed by the gradient-based Sobel edge detection algorithm and thresholded to identify the sudden dips of intensity or strong edges, which were correlated with the level of chromatin condensation. The thinning morphological algorithm was adopted to calculate the number of strong edges and generate an edge at the boundary of the nucleus, which was removed from all the identified edges. Further, the CCP was computed by dividing the number of edges by the nuclear area. The images of the nucleus were also processed by adjusting the threshold in ImageJ (NIH) following the reported

method(25). The adjusted threshold value was calculated by Mean of (0.4 * MAX) and MIN + (0.35* (MAX - MIN)), where MAX and MIN were the maximum and minimum nucleus fluorescent intensity, respectively. The adjusted image was re-coloured by red colour and then merged with the original nucleus image.

Immunofluorescence Staining. Corneal cells were seeded in confocal dishes (NEST Scientific USA) and fixed with 4% formaldehyde (Sigma Aldrich) for 15 min at room temperature. To block and permeabilize cells, 0.2% Triton X-100 (SAFC) in 1% bovine serum albumin (BSA) (VWR Life Science) was added for 1 h. The cells were then incubated with 1x Green Fluorescent Phalloidin Conjugate working solution (Abcam), diluted tubulin antibody (Sigma-Aldrich) or keratocan antibody for 1 h. Then the corresponding secondary antibody, Goat Anti-Rabbit IgG H&L (Alexa Fluor® 594) (Abcam) was added and incubated for 1 h at room temperature. At each step, cells were washed three times with PBS (Hyclone) to remove excess reagents. Finally, the cells were immersed in ProLong Gold Antifade Mountant with DAPI (Thermo Fisher Scientific) to counterstain the nucleus. For each condition, at least 40 cells were imaged by 63×/1.3 oil objective under the confocal microscope Leica DMi8 (Leica) in bright-field, fluorescein isothiocyanate (FITC), Rhod-2 and DAPI channels, respectively. Fluorescence intensity was quantified using ImageJ (NIH). In brief, the bright-field and fluorescent images of the same view were first stacked together by utilizing the Stack function in ImageJ software. The cell boundary was then identified in the bright-field image to calculate the cell area. The fluorescent intensity within the same cell boundary was measured under FITC or Rhod-2 channel in the fluorescent image. Therefore, the overall fluorescence intensity and spreading area of single cells were calculated. The mean fluorescence intensity (arbitrary unit: a.u.) was calculated through dividing the overall fluorescence intensity (integrated density function in ImageJ) by the cell area. For 3D confocal imaging, the images were taken every 0.5

μm in the direction of cell thickness and the reconstruction of 3D cell shape was conducted using the Leica software.

Statistical Analysis. All results were represented by mean ± standard error of the mean (SEM). The statistics between two conditions were analyzed by two-tailed Student's t-test. The ANOVA analysis was utilized for the statistics among three or more conditions. The post hoc Bonferroni test was adopted in the ANOVA analysis for the comparisons with unequal sample size.

Results

Corneal cells exhibit reduced F-actin/microtubule and cellular stiffness in high myopia

Cell cytoskeleton becomes remodeled under various pathologic conditions (26). To examine the association with myopia, we first explored the changes in the cytoskeleton of corneal cells in high myopia. High myopia was induced *in vivo* using two well-established paradigms, form-deprivation myopia (FDM) and lens-induced myopia (LIM) models, in the eyes of chicks as in *Experiment I* (Fig. 1a; Fig. S1a). Corneal tissues were extracted from both treated and control eyes and digested into single cell suspension. These chick-derived corneal cells were identified as keratocytes or fibroblasts, as they expressed the marker keratocan (Fig. S1b). The cytoskeleton of corneal cells was then examined by immunofluorescence staining, including F-actin and microtubule. The result shows that corneal cells from myopic eyes exhibited much lower levels of F-actin and microtubules than control cells (Fig. 1b and 1c; Fig. S2). The reduction of F-actin and microtubule during myopia progression was further confirmed using the LIM model (Fig. S1e and S1f). These findings suggest that corneal fibroblasts remodel their cytoskeleton significantly in high myopia.

Cytoskeleton is the structural basis of cell mechanics and its remodeling could induce alterations in cellular stiffness (26). To test this possibility, cellular stiffness was then quantified by AFM (27). Cellular stiffness is heterogeneous and highly depends on the probing location of the AFM tip, e.g., the nucleus is much stiffer than the cytoplasm (28). In this study, cellular area that was near the middle of the distance between the nucleus and cell periphery was chosen for stiffness measurement (Fig. S3), where average cell thickness was ~4.4 μm. Cells are intrinsically viscoelastic and usually assumed to be linear elastic under small strain (<10-15%) and low loading rate (1 μm/s) during the measurement (29), which was adopted in the current study. Cell stiffness was extracted from the measured force-deformation curve using the Sneddon's model under the hypothesis of linear elasticity (21). The result shows that myopic corneal cells exhibited significantly lower stiffness than control cells ($p<0.001$) (Fig. 1d and 1e). The histogram further illustrates that the stiffness distribution of corneal cells was shifted to the left during myopia progression (Fig. 1d). Similar findings of corneal fibroblast softening were also observed in high myopia using the LIM model (Fig. S1c and S1d). Since cell stiffness is closely associated with cytoskeleton (26), the reduction in cell stiffness may be explained by the decrease in F-actin/microtubule content. These findings suggest that corneal cells exhibit reduced cellular stiffness in high myopia.

Myopic corneal cells fully/partially restore F-actin/microtubule and mechanical stiffness to the levels of healthy cells after recovery into the healthy state

We next examined the changes in the cytoskeleton of corneal cells after recovery from high myopia into the healthy state. While form deprivation and minus lens-wear induced similar levels of high myopia in chicks (~-20 D) (Fig. 2a; Fig. S1a) as in *Experiment II* (Supporting Material), two days of unrestricted vision *in vivo* following these treatments reduced the myopia level by 78.8% (-5 D) and 48.8% (-9 D), respectively (Fig. 2b; Fig. S4a), indicating

that the treated eyes had partially recovered into the healthy state. The result shows that there was no significant difference in F-actin between myopic cells after recovery and control corneal cells (Fig. 2c; Fig. S5a-b), while microtubules were partially reinstated (Fig. 2d; Fig. S5c-d), suggesting that the cytoskeleton of myopic cells is partially restored to a level similar to that of control cells after recovery. Similarly, myopic corneal cells exhibited significantly lower stiffness than healthy ones (Fig. 2e). Strikingly, when myopia was recovered within two days *in vivo* to the healthy state, the stiffness of myopic corneal cells was restored to the level of control cells ($p=0.795$ in Fig. 2f), which could be clearly seen in the distribution of cellular stiffness (Fig. 2g). Further, the results from the LIM model also showed similar patterns of changes in the cytoskeleton and cellular stiffness, in which F-actin and microtubules were fully reinstated after only two days of recovery (Fig. S4b-e). The reinstatement of cell cytoskeleton in myopic corneal cells after recovery supports the restoration of cell stiffness in recovered corneal cells. Previous research shows that cytoskeleton plays an important role in corneal fibroblast morphology and contractility in 3D collagen (30). On the other hand, limbal epithelial cells are softer than their differentiated counterparts on 2D substrates, while there is no significant difference in cell aspect ratio or morphology (18). Therefore, the relationship between cytoskeleton, cell morphology, and mechanical behavior seems to be more complex than expected. In this study, although there were significant differences in cytoskeleton and cell stiffness between control and myopic cells and between myopic cells and recovered cells, cell aspect ratio and spreading area were similar among control, myopic, and recovered corneal cells (Fig. S6). These suggest that the interaction between different cytoskeletal elements and cytoskeleton-related proteins may be involved in addition to cytoskeletal remodeling (31). However, the underlying mechanism remains unclear. Collectively, these results suggest that only short period of recovery can restore F-actin and stiffness and partially restore microtubule of myopic corneal cells to the levels of healthy cells.

Myopic corneal cells generate enhanced traction force that is restored to the level of control cells after recovery

Living cells actively generate contractile force that influences various cellular functions but is difficult to be measured directly (32). Since contractile force is transmitted to the underlying substrate through cell-substratum interface, traction force exerted on the substrate is usually utilized to estimate the intracellular contractile force (33). We next examined the levels of traction force of corneal cells under normal, myopic, and recovered conditions in both FDM and LIM models through traction force microscopy (22, 23). The results from the FDM model show that the traction force generated by myopic corneal cells was significantly higher than that of control cells (Fig. 3a and 3b), suggesting that corneal cells may remodel the cytoskeletal elements and activate the Rho-ROCK-myosin signaling (26). Importantly, after the treated eyes were allowed to recover to the healthy state, the traction force generated by the recovered corneal cells was reduced to a level similar to control cells (Fig. 3c and 3d). Similar findings were also found in the LIM model (Fig. S7). These findings suggest that cellular contractility is elevated in high myopia condition and restored to the level of healthy cells after recovery, demonstrating the association between myopia and cellular contractile force.

Myopic corneal cells exhibit enhanced chromatin condensation that is restored to the level of control cells after recovery

All the chromosomes are packed in a small nucleus with certain level of chromatin condensation, which is usually altered under pathologic conditions and may regulate the transcription of related genes and thus influence various cellular functions (34). Aberrant chromatin structure and condensation level mediate the dysregulation of gene transcription programme, which leads to many pathologic processes (35). Therefore, we further examined the level of chromatin condensation in high myopia. In the cell nucleus, the density of

heterochromatin increases when cells undergo chromatin condensation and can be detected by the gradient-based Sobel edge detection algorithm. As a measure of chromatin condensation level, chromatin condensation parameter (CCP), defined as the density of edges within the nucleus divided by nuclear area (36), was adopted to evaluate chromatin compaction . The results from the FDM model showed that there was a significant increase in nuclear edge density within the nucleus of myopic corneal cells compared with control cells (Fig. 4a and 4b), suggesting that the nuclei of myopic corneal fibroblasts exhibit a higher level of chromatin condensation. The level of chromatin condensation in myopic cells was restored to a level similar to that in control cells after recovery into the healthy state (Fig. 4c and 4d). Similar results were also observed in the LIM model (Fig. S8). These results demonstrate that chromatin condensation is enhanced in myopic corneal cells and restored to the level of control cells after recovery.

Discussion

Emerging evidence has demonstrated that significant alterations in the structural and biomechanical properties of corneal tissue are correlated with myopia progression both in humans (15, 37, 38) and animals (14, 39). The deformability or the softness of cornea is positively correlated with the level of myopia (40). Our previous work has shown that the tangential modulus of the cornea is moderately compromised in highly myopic chicks (14). Although the reduction in corneal tissue stiffness has been hypothesized to be involved in myopia, it is still unclear how corneal mechanical strength is altered during myopia progression. The current study has shown that corneal fibroblasts are significantly softened in high myopia in both FDM and LIM chick models. The decrease in corneal cell stiffness is correlated with the reduced F-actin and microtubules in myopic cells, and the increase in cell stiffness after recovery is accompanied by the full/partial restoration of F-actin/microtubule to the level of

control cells. These findings suggest that the alteration in cell stiffness during myopia progression may be attributed to the remodeled cytoskeleton, as cytoskeletal structure plays critical roles in determining cell mechanics (26). Recent evidence shows that the interaction between actomyosin and microtubule affects cell protrusion and migration (41, 42) and possibly influences cell mechanics. Due to their importance in cytoskeletal remodeling and cellular stiffness, cytoskeleton proteins (e.g., α-actinin, filamin A, Arp2/3, etc) possibly contribute to the changes in the mechanics of corneal fibroblasts during myopia progression. The cytoskeletal remodeling and the reduction in fibroblast stiffness may influence cellular functions, including generating elevated contractile forces (43) and possibly decreasing the synthesis of collagen crosslinker lysyl oxidase and deposition of collagen (44), which may lead to corneal tissue weakening. Further efforts are needed to investigate the role of corneal cell mechanics in tissue biomechanics. In addition, traction force is related to cell migration (45). The difference in the generated traction force between normal and myopic corneal cells may suggest their differential migration ability. Importantly, the stiffness of corneal cells is restored to the normal level after myopic eyes recover to the healthy state, suggesting that corneal cell biomechanical change is reversible and thus serves as a mechanical indicator of myopia. Nevertheless, it is worthy to further investigate the dynamic changes of corneal cell mechanics at different levels of myopia and the significance of these biophysical alterations in myopia progression.

Since chromatin regulation impacts gene transcription and various cellular functions, the aberrant chromatin condensation/de-condensation is involved in many pathologic processes (35). The current study has demonstrated that the level of chromatin condensation is reversibly changed during myopia progression and recovery, suggesting that this dynamic alteration in chromatin compaction may influence the transcription of certain genes that are important in myopia and further contribute to the progression of this ocular disorder. To test this possibility,

it is critical to explore the role of the dynamic chromatin condensation in myopia and the underlying molecular mechanisms, including the regulation of genes that are essential in myopia progression. In addition, it would be interesting to examine the relationship between cellular biophysical changes and chromatin condensation and address whether they function synergistically or independently in myopia. Further, the findings of this study are based on well-established chick myopia models. Despite the similarities in anatomical composition (46, 47) and relative thickness (48)of the chicken and human cornea, the former is capable of altering its corneal curvature for extra dioptric power (49, 50), suggesting different mechanical requirements between these two species. Therefore, one should be cautious when extending the findings in chicks to myopia progression in human.

AFM has been widely used to probe cellular stiffness by indenting local cell areas, from which the relationship between the probing force and the induced cell deformation can be obtained. Theoretical models are required to extract cell elastic modulus from the force-deformation curve, including Sneddon's model, in which a finite indenter is assumed to interact with a semi-finite, homogenous, and elastic sample. Although Sneddon model has been widely adopted to obtain cell stiffness in AFM measurement, one should be cautious about the assumptions and thus the limitations of this model. The model assumes that a cell is homogeneous, isotropic, and linear elastic, which may not faithfully recapitulate the cell complexity, since living cells are intrinsically heterogeneous, anisotropic, and viscoelastic. Further, biological materials usually exhibit strain-dependent (strain-hardening or softening) mechanical properties, which are not considered in Sneddon model. In the lateral direction, the cell size is around 20-40 μm, which is far larger than the tip size (20-50 nm). In the vertical direction, when the biological sample is indented by more than 15% of the thickness, the effect from the underlying substrate needs to be considered and nonlinear elasticity should be assumed (51, 52). In this study, the average thickness of the probed cell area is 4.4 μm, while the indentation depth is 500 nm.

Therefore, it is reasonable to neglect the substrate effect and assume the linear elasticity of cells. Nevertheless, the main sources of error in the stiffness measurement by AFM may include the uncertainty in the calibration of tip deflection sensitivity and cantilever's spring constant as well as the adopted theoretical model, including the assumption of linear elasticity and infinite cell sample (53). In addition, it took almost one hour to collect corneal tissues after euthanasia and another hour to extract single cells from the corneal tissue in this study. We assume that the possible post-mortem effect on cytoskeletal re-organisation and mechanics could be minimal or similar among different conditions so that it would not impact the general conclusion that corneal keratocytes become softened and more contractile during myopia progression that can be restored to the levels of healthy cells after recovery.

Conclusion

In summary, this study demonstrates that myopic corneal cells exhibit reduced F-actin/microtubule and cellular stiffness while generate enhanced traction force and exhibit higher levels of chromatin condensation in the nucleus compared to healthy cells. After recovery to the healthy state, the biophysical phenotype and chromatin condensation of myopic cells are fully/partially restored to the levels of healthy cells. These findings suggest that the biophysical properties of corneal cells are correlated with myopia progression and may serve as a mechanical indicator for this ocular disorder. These observations facilitate the study of how biophysical alterations of corneal cells influence myopia at the cellular level.

Supporting Material

8 supplementary figures and 2 customized Matlab codes are available in the Supporting Material.

Author Contributions

Y.T. and C-S.K. conceived the project. Y.T., C-S.K., Y-P.Z., Y.X., B.S.K., and S.W.S. designed and conducted the experiments, and analyzed the data. Y.T., C-S.K., Y-P.Z., Y.X., and B.S.K wrote the manuscript. All authors commented and approved the manuscript.

Acknowledgments

We thank Dr. Maureen Valerie Boost from the Hong Kong Polytechnic University for critical reading of the manuscript and the University Life Science Facility in the Hong Kong Polytechnic University for providing confocal laser scanning microscopy and central animal facility. The authors acknowledge the support from National Natural Science Foundation of China (Project no. 11672255 and 11972316), Shenzhen Science and Technology Innovation Commission (Project no. JCYJ20170413154735522 and JCYJ20200109142001798), Early Career Scheme from Research Grants Council of the Hong Kong Special Administrative Region, China (PolyU 252094/17E), General Research Fund from Research Grants Council of the Hong Kong Special Administrative Region, China (PolyU 151004/18M and 15214320), and the Project of Strategic Importance of the Hong Kong Polytechnic University (1-ZE1A).

The authors declare no conflicts of interest.

References

1. Kempen, J. H.P. Mitchell et al.,. 2004. The prevalence of refractive errors among adults in the United States, Western Europe, and Australia. Arch. Ophthalmol. 122(4):495-505.
2. Holden, B.P. Sankaridurg et al.,. 2014. Myopia, an underrated global challenge to vision: where the current data takes us on myopia control. Eye (Lond.) 28(2):142-146.
3. Meng, W.J. Butterworth et al.,. 2011. Axial length of myopia: a review of current research. Ophthalmologica 225(3):127-134.
4. Flitcroft, D. I.M. He et al.,. 2019. IMI - Defining and Classifying Myopia: A Proposed Set of Standards for Clinical and Epidemiologic Studies. Invest. Ophthalmol. Vis. Sci. 60(3):M20-m30.

5. Troilo, D. E. L. Smith, 3rd et al.,. 2019. IMI - Report on Experimental Models of Emmetropization and Myopia. Invest. Ophthalmol. Vis. Sci. 60(3):M31-m88.
6. Isermann, P.J. Lammerding. 2013. Nuclear mechanics and mechanotransduction in health and disease. Curr. Biol. 23(24):R1113-1121.
7. Ingber, D. E. 2003. Mechanobiology and diseases of mechanotransduction. Ann. Med. 35(8):564-577.
8. Tan, J. C.F. B. Kalapesi et al.,. 2006. Mechanosensitivity and the eye: cells coping with the pressure. Br. J. Ophthalmol. 90(3):383-388.
9. Suresh, S. 2007. Biomechanics and biophysics of cancer cells. Acta Biomater. 3(4):413-438.
10. Tan, Y.T.-K. Fung et al.,. 2011. Biophysical characterization of hematopoietic cells from normal and leukemic sources with distinct primitiveness. Appl. Phys. Lett. 99(8):083702.
11. Suresh, S.J. Spatz et al.,. 2005. Connections between single-cell biomechanics and human disease states: gastrointestinal cancer and malaria. Acta Biomater. 1(1):15-30.
12. Hahn, C.M. A. Schwartz. 2009. Mechanotransduction in vascular physiology and atherogenesis. Nat. Rev. Mol. Cell Biol. 10(1):53-62.
13. Jaalouk, D. E.J. Lammerding. 2009. Mechanotransduction gone awry. Nat. Rev. Mol. Cell Biol. 10(1):63-73.
14. Kang, B. S.L. K. Wang et al.,. 2018. High myopia induced by form deprivation is associated with altered corneal biomechanical properties in chicks. PLoS One 13(11):e0207189.
15. He, M.W. Wang et al.,. 2017. Corneal Biomechanical Properties in High Myopia Measured by Dynamic Scheimpflug Imaging Technology. Optom. Vis. Sci. 94(12):1074-1080.
16. Yu, A. Y.H. Shao et al.,. 2020. Corneal biomechanical properties in myopic eyes evaluated via Scheimpflug imaging. BMC Ophthalmol. 20(1):279.
17. Blackburn, B. J.M. W. Jenkins et al.,. 2019. A Review of Structural and Biomechanical Changes in the Cornea in Aging, Disease, and Photochemical Crosslinking. Front Bioeng Biotechnol 7:66.
18. Bongiorno, T.J. L. Chojnowski et al.,. 2016. Cellular Stiffness as a Novel Stemness Marker in the Corneal Limbus. Biophys. J. 111(8):1761-1772.
19. Maruri, D. P.M. Miron-Mendoza et al.,. 2020. ECM Stiffness Controls the Activation and Contractility of Corneal Keratocytes in Response to TGF-β1. Biophys. J. 119(9):1865-1877.
20. Kee, C. S.L. Deng. 2008. Astigmatism associated with experimentally induced myopia or hyperopia in chickens. Invest. Ophthalmol. Vis. Sci. 49(3):858-867.
21. Roy, R.J. P. Desai. 2014. Determination of mechanical properties of spatially heterogeneous breast tissue specimens using contact mode atomic force microscopy (AFM). Ann. Biomed. Eng. 42(9):1806-1822.
22. Liu, J.Y. Tan et al.,. 2012. Soft fibrin gels promote selection and growth of tumorigenic cells. Nat Mater 11(8):734-741.
23. Jin, J.K. Tang et al.,. 2018. Hemodynamic shear flow regulates biophysical characteristics and functions of circulating breast tumor cells reminiscent of brain metastasis. Soft Matter 14(47):9528-9533.
24. Irianto, J.D. A. Lee et al.,. 2014. Quantification of chromatin condensation level by image processing. Med. Eng. Phys. 36(3):412-417.
25. Damodaran, K.S. Venkatachalapathy et al.,. 2018. Compressive force induces reversible chromatin condensation and cell geometry-dependent transcriptional response. Mol. Biol. Cell 29(25):3039-3051.

26. Fletcher, D. A.R. D. Mullins. 2010. Cell mechanics and the cytoskeleton. Nature 463(7280):485-492.
27. Xin, Y.X. Chen et al.,. 2019. Mechanics and Actomyosin-Dependent Survival/Chemoresistance of Suspended Tumor Cells in Shear Flow. Biophys. J. 116(10):1803-1814.
28. Ofek, G.R. M. Natoli et al.,. 2009. In situ mechanical properties of the chondrocyte cytoplasm and nucleus. J. Biomech. 42(7):873-877.
29. Kontomaris, S. V.A. Stylianou et al.,. 2019. Determination of the linear elastic regime in AFM nanoindentation experiments on cells. Materials Research Express 6(11):115410.
30. Kim, A.W. Matthew Petroll. 2007. Microtubule regulation of corneal fibroblast morphology and mechanical activity in 3-D culture. Exp. Eye Res. 85(4):546-556.
31. Keren, K.Z. Pincus et al.,. 2008. Mechanism of shape determination in motile cells. Nature 453(7194):475-480.
32. Wozniak, M. A.C. S. Chen. 2009. Mechanotransduction in development: a growing role for contractility. Nat. Rev. Mol. Cell Biol. 10(1):34-43.
33. Dembo, M.Y. L. Wang. 1999. Stresses at the cell-to-substrate interface during locomotion of fibroblasts. Biophys. J. 76(4):2307-2316.
34. Martin, R. M.M. C. Cardoso. 2010. Chromatin condensation modulates access and binding of nuclear proteins. FASEB J. 24(4):1066-1072.
35. Mirabella, A. C.B. M. Foster et al.,. 2016. Chromatin deregulation in disease. Chromosoma 125(1):75-93.
36. Heo, S. J.S. D. Thorpe et al.,. 2015. Biophysical Regulation of Chromatin Architecture Instills a Mechanical Memory in Mesenchymal Stem Cells. Sci. Rep. 5:16895.
37. Shen, M.F. Fan et al.,. 2008. Biomechanical properties of the cornea in high myopia. Vision Res. 48(21):2167-2171.
38. Hon, Y.G. Z. Chen et al.,. 2017. High myopes have lower normalised corneal tangent moduli (less 'stiff' corneas) than low myopes. Ophthalmic Physiol. Opt. 37(1):42-50.
39. Jiang, Z.M. Shen et al.,. 2011. Association between corneal biomechanical properties and myopia in Chinese subjects. Eye (Lond.) 25(8):1083-1089.
40. Wang, J.Y. Li et al.,. 2015. Corneal Biomechanical Properties in Myopic Eyes Measured by a Dynamic Scheimpflug Analyzer. J Ophthalmol 2015:161869.
41. Shakiba, D.F. Alisafaei et al.,. 2020. The Balance between Actomyosin Contractility and Microtubule Polymerization Regulates Hierarchical Protrusions That Govern Efficient Fibroblast-Collagen Interactions. ACS Nano 14(7):7868-7879.
42. Wolf, K. J.P. Shukla et al.,. 2020. A mode of cell adhesion and migration facilitated by CD44-dependent microtentacles. Proc. Natl. Acad. Sci. U. S. A. 117(21):11432-11443.
43. Kraning-Rush, C. M.J. P. Califano et al.,. 2012. Cellular traction stresses increase with increasing metastatic potential. PLoS One 7(2):e32572.
44. O'Brart, D. P. 2014. Corneal collagen cross-linking: a review. J Optom 7(3):113-124.
45. Trepat, X.M. R. Wasserman et al.,. 2009. Physical forces during collective cell migration. Nature Physics 5(6):426-430.
46. Fowler, W. C.D. H. Chang et al.,. 2004. A new paradigm for corneal wound healing research: the white leghorn chicken (Gallus gallus domesticus). Curr. Eye Res. 28(4):241-250.
47. Wisely, C. E.J. A. Sayed et al.,. 2017. The chick eye in vision research: An excellent model for the study of ocular disease. Prog. Retin. Eye Res. 61:72-97.
48. Ritchey, E. R.K. Code et al.,. 2011. The chicken cornea as a model of wound healing and neuronal re-innervation. Mol. Vis. 17:2440-2454.

49. Glasser, A.D. Troilo et al.,. 1994. The mechanism of corneal accommodation in chicks. Vision Res. 34(12):1549-1566.
50. Chu, C. H.Y. Zhou et al.,. 2014. Bi-directional corneal accommodation in alert chicks with experimentally-induced astigmatism. Vision Res. 98:26-34.
51. Dimitriadis, E. K.F. Horkay et al.,. 2002. Determination of elastic moduli of thin layers of soft material using the atomic force microscope. Biophys. J. 82(5):2798-2810.
52. Daily, B.E. L. Elson et al.,. 1984. Cell poking. Determination of the elastic area compressibility modulus of the erythrocyte membrane. Biophys. J. 45(4):671-682.
53. Schillers, H. C. Rianna et al.,. 2017. Standardized Nanomechanical Atomic Force Microscopy Procedure (SNAP) for Measuring Soft and Biological Samples. Sci. Rep. 7(1):5117.

Figures

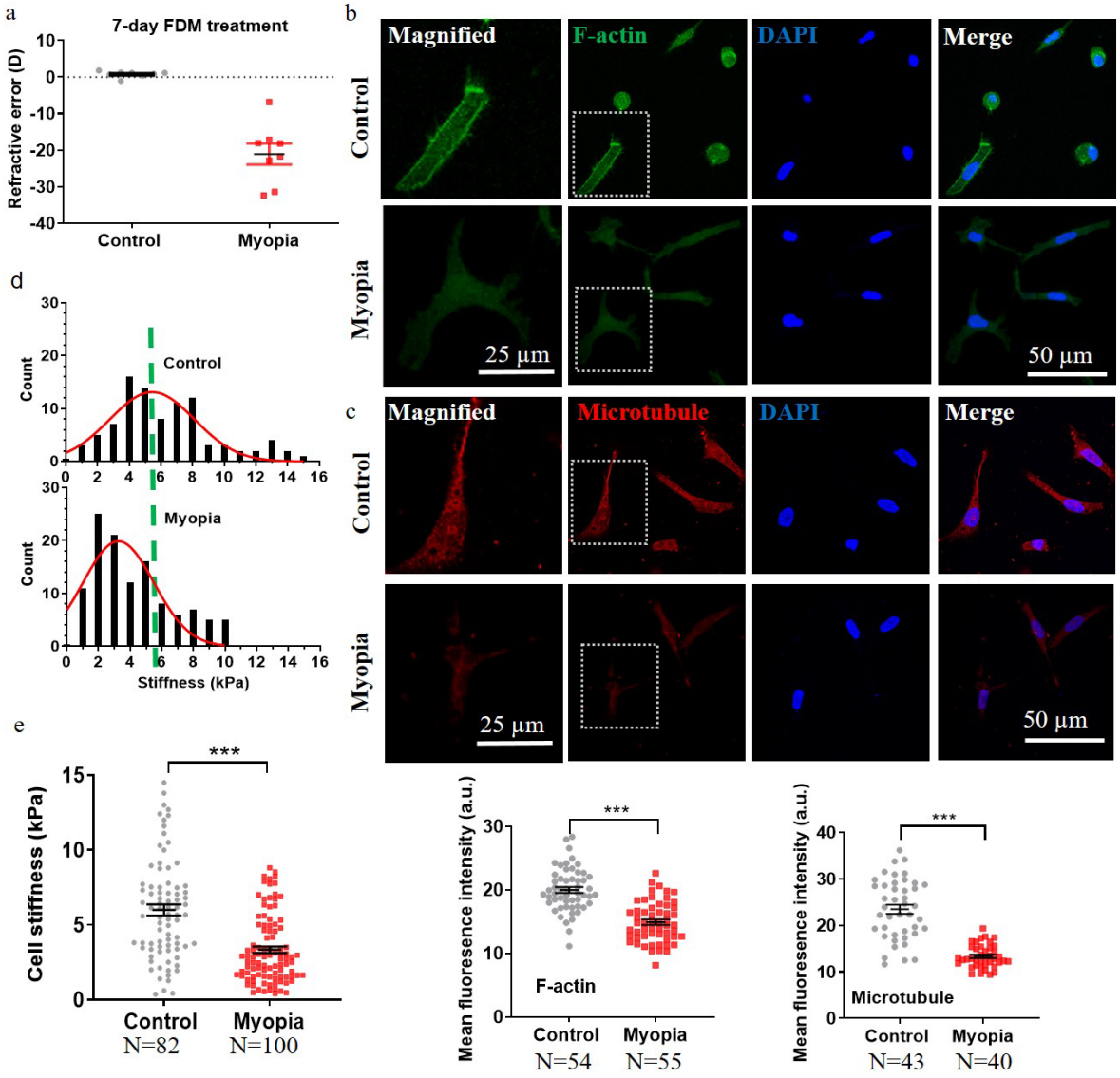

FIGURE 1 Myopic corneal cells exhibit reduced F-actin/microtubule and cellular stiffness. (a) Refractive state after the FDM treatment. Representative results of at least three independent experiments. (b, c) Myopic corneal cells exhibit lower levels of F-actin and microtubule than control cells. Single cells were extracted from the treated and fellow untreated control corneas in the FDM model. F-actin and microtubule were stained through immunofluorescence and the fluorescence intensity was quantified in the bottom panels. The cells in the dotted square were magnified on the left. Scale bar: 50 μm in the non-magnified images and 25 μm in the

magnified images. Representative results of three independent experiments. (d) The histogram of the stiffness of myopic corneal cells and control cells. The stiffness of myopic corneal cells and control cells was measured by AFM. (e) Myopic corneal cells are softer than control cells. n>80 cells. Representative results of three independent experiments. The number of cell samples was shown in the figures. ***, $p<0.001$.

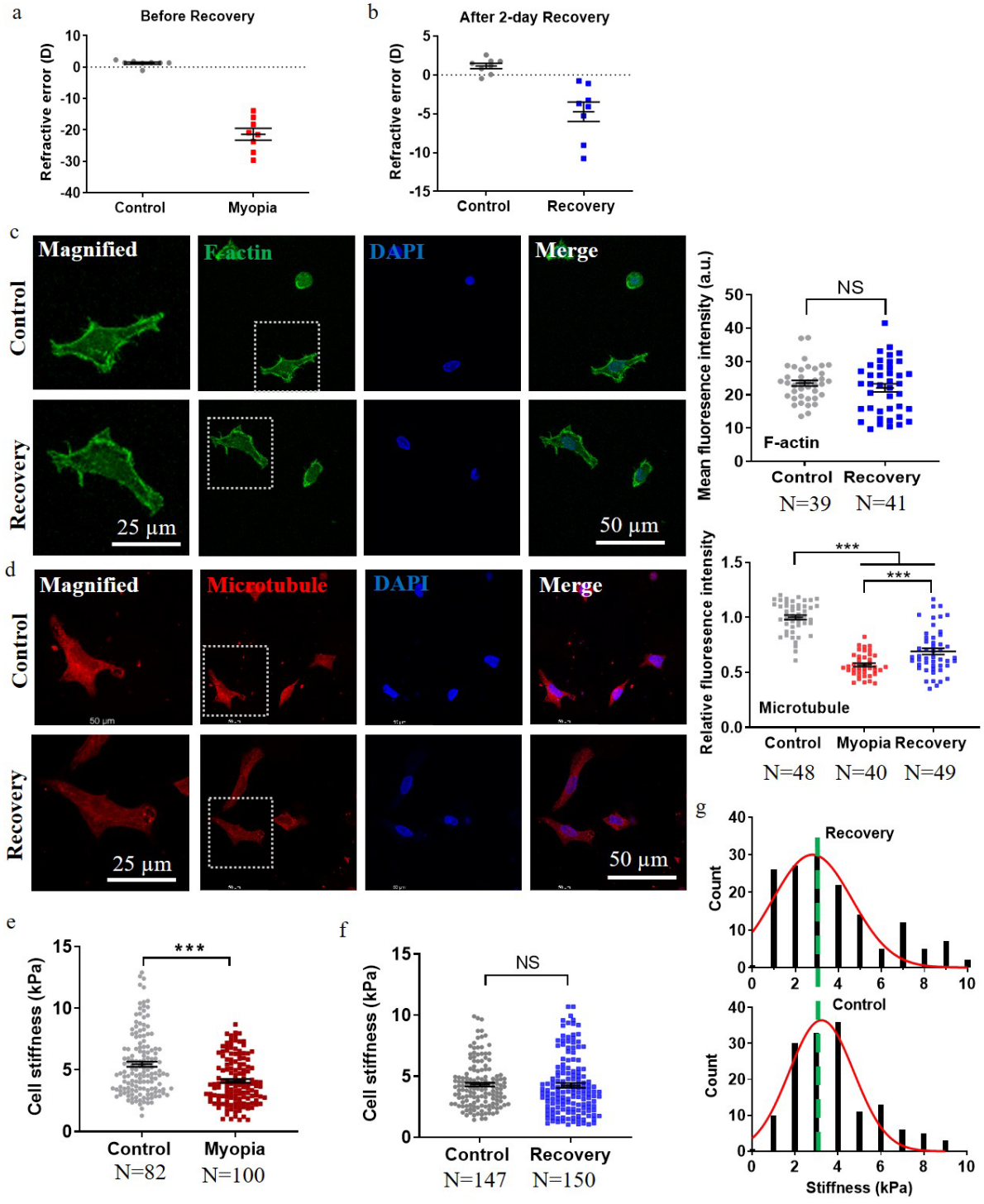

FIGURE 2 Myopic cells fully/partially restore F-actin/microtubule and cellular stiffness to the levels of control corneal cells after recovery to the healthy state. (a, b) The refractive state after the induction of myopia and recovery. Representative results of at least three independent experiments. (c, d) Recovered and control corneal cells restore F-actin and microtubule fully and partially, respectively. Single cells were extracted from the recovered and fellow untreated

control corneas in the FDM model. F-actin and microtubule were stained through immunofluorescence and the fluorescence intensity was quantified in the right panels. The cells in the dotted square were magnified on the left. Scale bar: 50 μm in the non-magnified images and 25 μm in the magnified images. Representative results of three independent experiments. (e) Myopic cells are soft than control corneal cells. Representative results of three independent experiments. (f) Recovered cells exhibit similar cellular stiffness to control corneal cells. Representative results of three independent experiments. (g) The histogram of cell stiffness in (f). The number of cell samples was shown in the figures. ***, $p<0.001$. NS: no significance.

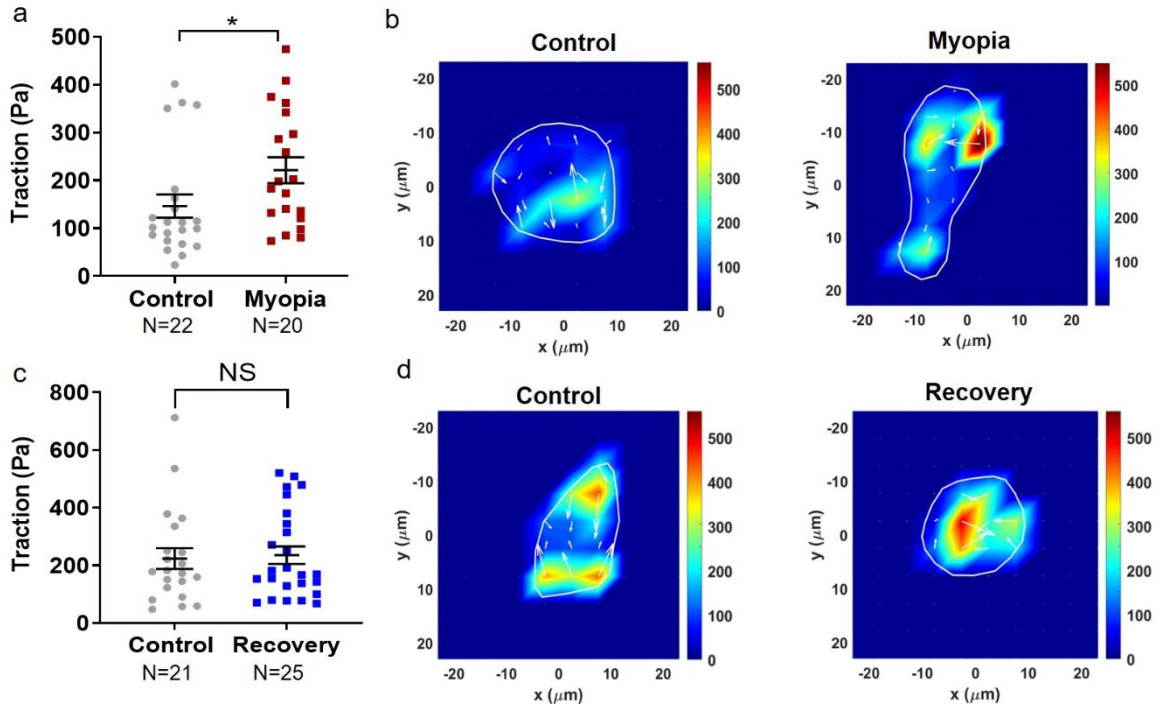

FIGURE 3 Myopic cells elevate traction force that is restored to the level of healthy corneal cells after recovery to the healthy state. (a) Myopic cells generate higher levels of traction force than control cells. The traction force of both myopic and control corneal cells was measured by traction force microscopy on 8 kPa polyacrylamide gels. n=3 independent experiments. *, $p<0.05$. (b) Representative images of traction forces in myopic and control cells. (c) Recovered cells generate similar traction force to control cells. n=3 independent experiments. NS: no

significance. (d) Representative images of traction forces in recovered and control cells. The number of cell samples was shown in the figures.

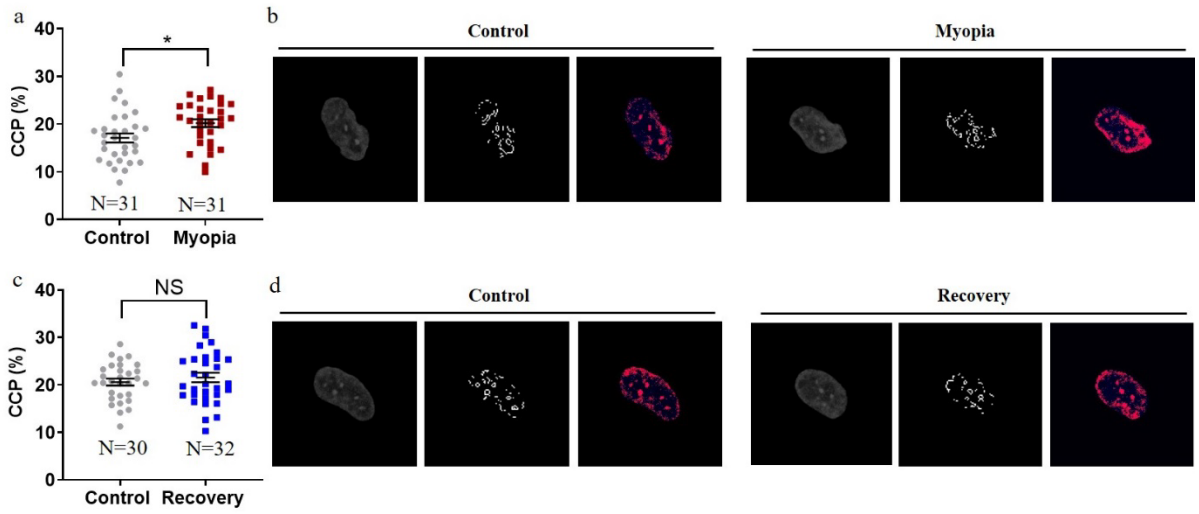

FIGURE 4 Myopic cells enhance chromatin condensation in the nucleus that is restored to the level of healthy corneal cells after recovery to the healthy state. (a) Myopic cells exhibit higher level of chromatin condensation than control cells. The chromatin condensation parameter (CCP) of both myopic and control corneal cells was measured by imaging processing to represent the level of chromatin condensation. Representative results of three independent experiments. *, $p<0.05$. (b) Representative images of chromatin condensation in myopic and control cells. The nuclei of both myopic corneal cells and control cells were stained with DAPI (left panel). The visible edges within the nucleus were identified by CCP image processing (middle panel) and the condensed nuclear area was filled with pseudo color (right panel). (c) Recovered cells exhibit similar level of chromatin condensation to control cells. Representative results of three independent experiments. NS: no significance. (d) Representative images of chromatin condensation in recovered and control cells. The number of cell samples was shown in the figures.